



HAL
open science

Dipolar self-assembled monolayers grafted on ZnO for the tuning of electronic properties of the poly (3-hexylthiophène)- [6,6]-phenyl C61-butyric acid methylester blend

Mariem Ben Youssef, Philippe Lang, Mahamadou Seydou, Faycal Kouki

► To cite this version:

Mariem Ben Youssef, Philippe Lang, Mahamadou Seydou, Faycal Kouki. Dipolar self-assembled monolayers grafted on ZnO for the tuning of electronic properties of the poly (3-hexylthiophène)-[6,6]-phenyl C61-butyric acid methylester blend. *Thin Solid Films*, 2020, 714, pp.138296. 10.1016/j.tsf.2020.138296 . hal-02996474

HAL Id: hal-02996474

<https://hal.science/hal-02996474>

Submitted on 9 Nov 2020

HAL is a multi-disciplinary open access archive for the deposit and dissemination of scientific research documents, whether they are published or not. The documents may come from teaching and research institutions in France or abroad, or from public or private research centers.

L'archive ouverte pluridisciplinaire **HAL**, est destinée au dépôt et à la diffusion de documents scientifiques de niveau recherche, publiés ou non, émanant des établissements d'enseignement et de recherche français ou étrangers, des laboratoires publics ou privés.

Dipolar Self-assembled Monolayers grafted on ZnO for the tuning of electronic properties of the poly (3-hexylthiophène)- [6,6]-phenyl C61-butyric acid methylester blend

Mariam Ben Youssef ^(a), Philippe Lang^{*(a)}, Mahamadou Seydou^(a) , Faycal Kouki^{*(b)}

^(a) ITODYS (UMR 7086), University of Paris (Paris 7), 15 rue Jean-Antoine de Baïf, 75205 Paris Cedex 13, France

* faycal_kouki@yahoo.fr ; lang@u-paris.fr

^(b) LMAPQ, Faculté des Sciences de Tunis, University Tunis El-Manar, 2092 El-Manar, Tunis, Tunisia

Abstract

A promising solution to improve the performance of Bulk heterojunction organic photovoltaic devices is the insertion of functionalized self-assembled monolayers (SAMs) at the interface between the Electron Transporting Layer (ETL) and the active layer. By grafting such dipolar SAMs based on Y-PP-COOH (P = Phenyl, Y = CH₃O, F) on a ZnO ETL, both the electronic and the chemical properties of the interface are modified. The growth of the active blend the poly(3-hexylthiophène)- [6,6]-phenyl C61-butyric acid methylester blend deposited onto the SAMs is also altered. The dipole with a component oriented perpendicularly to the ZnO surface modifies the ZnO work function whereas the surface energy of the SAM influences the microstructuration of the active material. When we analyze the inverted photovoltaic cell, we find that the two effects may be distinguished: the CH₃O moiety favorably affects the electrical transfer of carriers with mainly an improvement of the open-circuit voltage V_{oc} whereas fluorine disfavors both electron extraction and blend microstructure quality, with a lower V_{oc} and electrical current density J_{sc} .

1. Introduction

Organic solar cells (OSCs) based on π -conjugated semiconducting (SC) polymers are becoming potential alternative candidates in the field of photovoltaic conversion since they can be fabricated by cost-effective large-area printing and coating processes on top of flexible substrates [1-3]. Bulk heterojunction (BHJ) solar cells, based on π -conjugated polymers and fullerene-derivative blend layers sandwiched between a transparent conducting electrode, namely Fluoride Tin Oxide (FTO) and a low-work-function metal electrode, have proven to be worthy competitors to polycrystalline silicon-based cells [4-6]. Over the past few years, important results have shown that the performance of OSCs can be enhanced by the development of materials and/or the optimization of morphologies by processing methods [7-10]. The photoinduced charge separation, the charge transport and the collection properties govern the performances of OSCs, yet one of the most crucial parameters in the photogeneration process is the built-in electric field, the strength of which is strongly dependent on the energy levels of the anode and cathode electrodes.

The development of Organic Photovoltaic (OPV) still faces the limitation of relatively low yields compared to mineral photovoltaic cells. This limitation is attributable to the very nature of the photogeneration process in OPVs. Indeed, the absorption of light by these materials leads to the creation of geminate electron-hole pairs, commonly called excitons, whose Bohr radius depends essentially on the dielectric constant of the material. Given its low value in organics ($\epsilon = 3$), this results in too high a binding energy, which makes dissociation of the geminate electron-hole pairs into two free carriers difficult.

Efforts to overcome this major drawback have mainly focused on the design of the heterostructures of the Donor/Acceptor blend type Bulk HeteroJunctions (BHJ) [11,12]. The other important limitation concerns the metal/active-layer interfaces. Electrical contacts ensuring the collection and delivery of photogenerated charges are important to the operation of these cells. Indeed, the energy levels of the anode (high work function electrode) and the cathode (low work function electrode) determine the performance of the OSCs. Subsequently, the formation of these interfaces must not generate either a potential barrier, which would inhibit the flow of charges, or energy losses. Moreover, the difference in their work functions should

be as large as possible, in order to ensure the presence of the indispensable intrinsic electric field within the active layer. So, to ensure an efficient selective carrier flow, i.e. inhibiting the flow of electrons towards the anode and the flow of holes toward the cathode, layers of metal oxide (MOx) with appropriate energy levels are deposited onto metal electrodes or transparent conductive oxides. Nevertheless, these intermediate layers are found to be inefficient, because of the presence of surface states and insufficient alignment of their electronic levels with the active component. Within this context, we aim to control the physic chemistry of the interface at the level of the electrodes by functionalization by self-assembled dipolar layers whose purpose is to control the alignment of the electronic levels as well as the structure of the active layers.

Thin ZnO layers in the inverted architecture have been widely used as Electron Transport Layer (ETL) in recent years [13-16]. This structure is found to be much more stable, since the final coating layers are less sensitive to oxidation from air, which in turn improves the stability and therefore the performance of the OPV cells [17-21]. This approach requires reverse-order deposition of the layers, making it possible to use the most stable metals, such as Au and Ag, as hole-collection electrodes [22].

The grafting of dipolar Self-Assembled Monolayers (SAMs) on top of ZnO layers turned out to be an efficient way of aligning the electronic levels of the oxides and those of the active materials in order to avoid energy losses and extraction barriers. In addition, SAMs thanks to their adequate terminal function, allow the control of chemical properties and energy of the surface where the SC is then deposited. When the dipole moment is directed from the organic semiconductor (SC) to the ETL, the level of the ZnO conduction band, close to the Fermi level with an n-doped oxide, is pushed up relative to the Lower Unoccupied Molecular Orbital (LUMO) of the acceptor, with a change of the work function of the transport layer, δW (Fig. 1). For hole transport layer the valence bands are concerned. The ideal situation corresponds to the alignment of the conduction band (CB) and the LUMO (Fig. 1) or the valence band (VB) with the Highest Occupied Molecular Orbital (HOMO) (p-type oxide and acceptor). The electrons flow therefore from the LUMO of the donor to the CB of the ETL without losing energy.

Others surface treatments have been proposed in this goal sometimes easier to perform without the driving of the surface chemical properties [23,24]

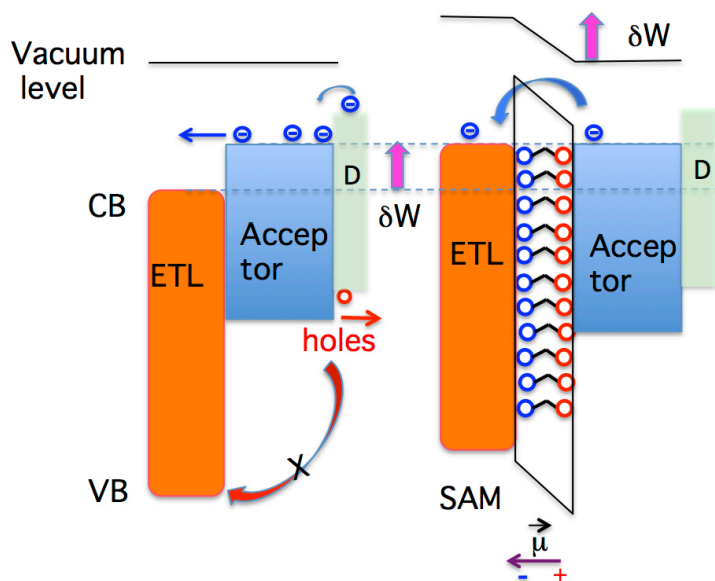


Figure 1. Principle of the alignment of the LUMO of a acceptor with the CB of the ETL via a dipolar SAM to reduce energy losses at the interfaces of a solar cell. (D is the donor)

The grafting of SAMs onto ZnO bearing phosphoric and carboxylic acid functions is efficient, as reported in previous work [25-27]; they form stable bonds and lead to uniform coverage.

In this work, we analyze the effect of the functionalization of the surface of ZnO, by grafting self-assembled dipolar molecules of general structure para-Y-PP-COOH (YA), on the performance of an inverted solar cell. PP is a biphenyl spacer and Y is either an electron withdrawing ($Y = F$) or donating ($Y = OCH_3$) group. Both the structure of the ZnO layer, the grafting and the orientation of the SAM on the ZnO layer were analyzed by IR Spectroscopy, X ray diffraction (XRD) and contact angle measurements. In order to highlight and enhance the effect of two F- and CH_3O - terminated SAMs alone (F-A and CH_3O -A, respectively), no additives were added to the blend and no advanced optimization of the device was performed. Only the oxide synthesis, cleaning and dipolar molecule adsorption conditions were optimized.

2. Experimental procedure

Materials: 4-(4'-Fluorophenyl)benzoic acid (F-PP-COOH = F-A) and 4'-methoxybiphenyl-4-carboxylic acid CH_3O -PP-COOH (noted CH_3O -A) were purchased from Alfa-Aesar and Aldrich, respectively, and were used as received unless stated otherwise. Regioregular poly(3-hexylthiophene) (P3HT) and phenyl-C60-butyric acid methyl ester (PCBM) were purchased from Aldrich.

Synthesis of ZnO nanoparticles (NP): $Zn(CH_3COO)_2$ (2.2 g; 0.01 mol), diethylene glycol (98.2 ml) and ultrapure H_2O (1.8 ml, 0.1 mol) were mixed in a three-necked flask, and the mixture refluxed at 180 °C with stirring for 1 hour. After cooling, the product was

centrifuged 3 times with absolute ethanol [28,29].

The obtained NPs were cylinder-shaped with an average particle size of about 30 nm (Fig. 2). A 200 nm-thick sample was prepared and characterized by XRD. As shown in Figure 3, we observe clearly a hexagonal crystal system for ZnO NPs, as described in the literature.

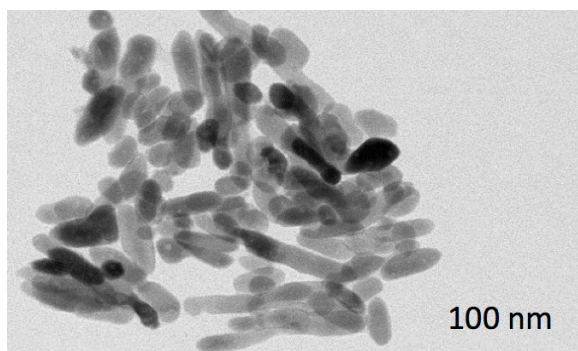


Figure 2: TEM image of ZnO nanoparticles synthesized by polyol way

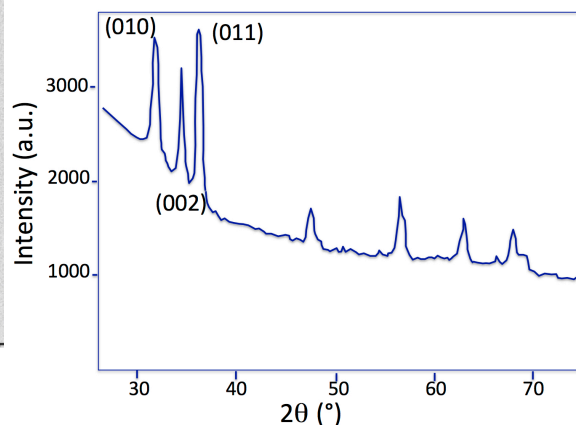


Figure 3: XRD pattern of ZnO NP with hexagonal crystal system $\alpha=\beta=90^\circ$; $\gamma=120^\circ$ $a=b\neq c$

Fabrication of OSCs: For the fabrication of OSCs, a 30 nm-thick layer of ZnO film on treated FTO (sheet resistance = 15 ohm/square, 2×2 cm²) was spin-coated onto FTO at 6000 rpm for 30 s and then annealed at 100 °C for 5 min. The ZnO layer is treated with a RCA mixture (H₂O₂;NH₃;H₂O in a ratio of 1/1/1600 v/v) at 80 °C for 10 min. The adsorption of SAMs on ZnO from CH₂Cl₂ solutions (5.10^{-4} M) was accomplished by dipping the sample for 2 hours. The blend solution of P3HT (Donor) –PCBM (acceptor) was dissolved in dichlorobenzene at a concentration of 25 mg/ml (1:1) and was spin-coated at 1500 rpm for 60 s on FTO. The typical thickness of the active layer was 150 nm. Before the final coating with PEDOT:PSS/Au, the active layer was thermally annealed at 150 °C for 20 min. Finally a 100 nm-thick Au electrode was vacuum-deposited at 2×10^{-4} Pa on top of the spin-coated PEDOT:PSS through a shadow mask. The active pixels obtained have an area of approximately 0.2 cm².

Measurements: The orientation of the two grafted molecules, F-A and CH₃O-A, deposited on ZnO/Au were characterized by Polarization Modulation-Infrared Reflection-Absorption Spectroscopy (PM-IRRAS) measurements using a Nicolet 8700 spectrometer (sum of 2000 scans, 4 cm⁻¹ resolution, and 0.47 cm⁻¹ optical velocity) along with a photoelastic modulator PEM-90 (Hind Instruments). To obtain the selection rule, ZnO was deposited on flat Au substrates.

The surface energy (γ) of the ZnO layer before and after SAM treatment was evaluated by measurement of the static advancing contact angle with deionized water and diiodomethane. The contact angles (Kruss, Model DSA 25) were entered into the Wu model (harmonic mean) for the calculation of the dispersive and polar components of the surface energy. Current density-Potential (J-V) measurements under illumination (65 mW/cm^2) by a Xe lamp (150 W) with a 1.5 G filter were performed using a Keithley model 2400 source measure unit.

Quantum chemical calculations: The optimizations and analytical frequency calculations were conducted by using density functional theory (DFT) at B3LYP/6-31+G* level of theory as implemented in Gaussian09 [30]. The corresponding infrared absorption spectra have been simulated from calculated frequencies with the recommended uniform scaling factor of 0.9614 [31]. The values of dipole moments of CH₃O-PP-COOH and of F-PP-COOH along the z-axis are 2.94 D and 0.15 D. (Fig.4) . The values of dipole moments of CH₃O-PP-COOH and of F-PP-COOH along the z-axis are 2.94 D and 0.15 D. (Fig.4)

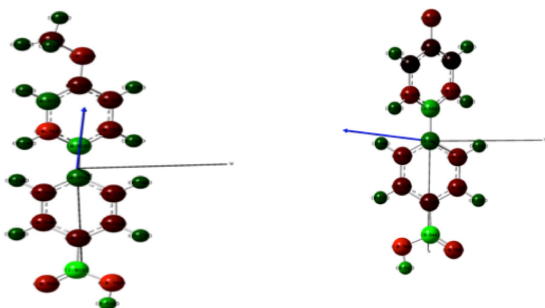


Figure 4: calculation of dipolar moment of CH₃O-PP-COOH and F-PP-COOH

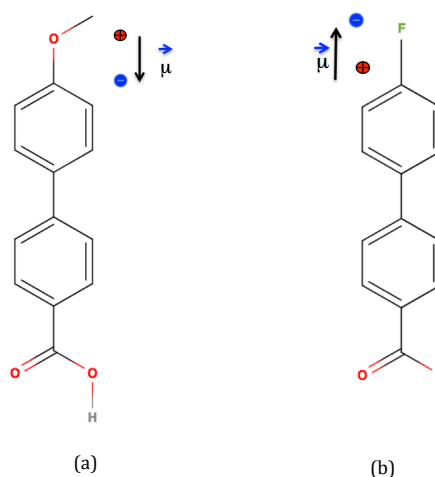


Figure 5. Chemical structures: (a) CH₃O-A; (b) F-A and the dipole induced by the terminal moiety.

3. Grafting and structure of the dipolar SAMs onto ZnO layer

We used two different molecules Y-PP-COOH (Y = F, OCH₃) bearing an electron-withdrawing (Y = F) or donating (Y = OCH₃) substituent. As shown in Figure 5, the dipole moment of grafted molecules assembled in a monolayer is a priori expected to point towards the substrate for CH₃O-PP-COOH (CH₃O-A) whereas that for F-PP-COOH (F-A) points towards the bulk of the active layer.

Vibrations and their polarization (L, M, N)	molecule grafted onto ZnO/Au; PM-IRRAS (cm ⁻¹)		molecule grafted on ZnO NP in KBr (cm ⁻¹)		Molecule in KBr (cm ⁻¹)			
	F-A	CH3O-A	F-A	CH3O-A	F-A		CH3O-A	
					Cal.	Exp.	Cal.	Exp.
$\nu(\text{C=OOH})$					1719	1689	1716	1681
$\nu(\text{COO}^-)_{\text{as}}$	1542	1545	1540	1549				
$\nu(\text{COO}^-)_{\text{s}}$	1424	1426	1431	1425				
Phenyl ν_1 , (L)	1605	1606	1603	1606	1596	1609	1589	1599
Phenyl ν_2 , (M)	1525		1525	1526	1545	1525	1538	1530
$\nu(\text{OC-OH})$		1255		1256			1320	1328
$\nu(\text{C-F})$	1244		1243		1208	1240		
$\gamma(\text{C-H})$ (N)	833	831	834	831	815	824	813	831

Table 1. Assignment and wavenumbers of the main bands for F-A and CH3O-A in KBr, grafted onto ZnO NPs/Au in KBr, and calculated values.

3.1. Characterization by infrared spectroscopy

3.1.1. Assignment of bands by the DFT method

In a first step, we are interested in indexing the IR bands of CH₃O-A and F-A in KBr pellets. This attribution was determined with the help of calculated frequencies.

For CH₃O-A the calculated bands were assigned as follows: the carboxylic acid band COOH at 1716 cm⁻¹; the band at 1589 cm⁻¹ corresponds to the band of L-polarized phenyl (ν_1); the band of the M-polarized phenyl (ν_2) is at 1538 cm⁻¹. In the low wavenumber region, the band at 813 cm⁻¹ was assigned to the C-H out-of-plane vibration (N-polarized) (Table 1, Fig. 6-7).

Similarly, for F-A the attributions of the bands can be determined. For high wavenumbers, the band at 1719 cm^{-1} was assigned to the carboxylic acid band COOH. For the phenyl bands, the first band ν_1 (C=C) located at 1596 cm^{-1} is L-polarized and the second, ν_2 (C=C), at 1545 cm^{-1} is M-polarized. The out-of-plane vibration C-H band of the biphenyl moiety at 810 cm^{-1} is N-polarized .

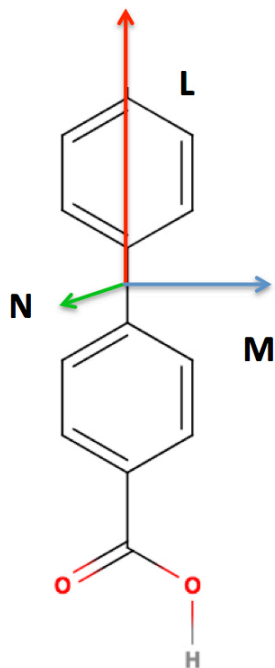


Figure 6. Polarization axis L, M, N or direction of the possible transition dipolar moment of the Y- PP-COOH molecule (Y not represented)

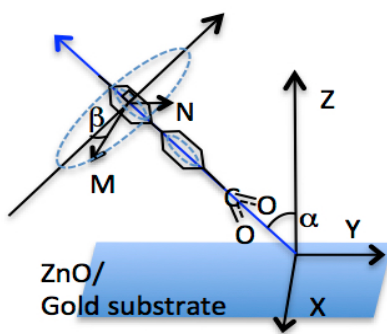
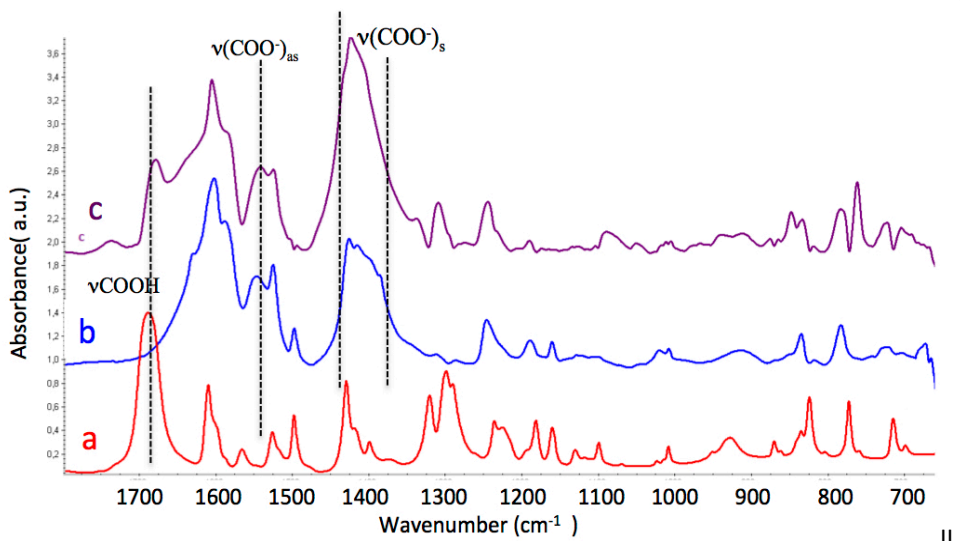
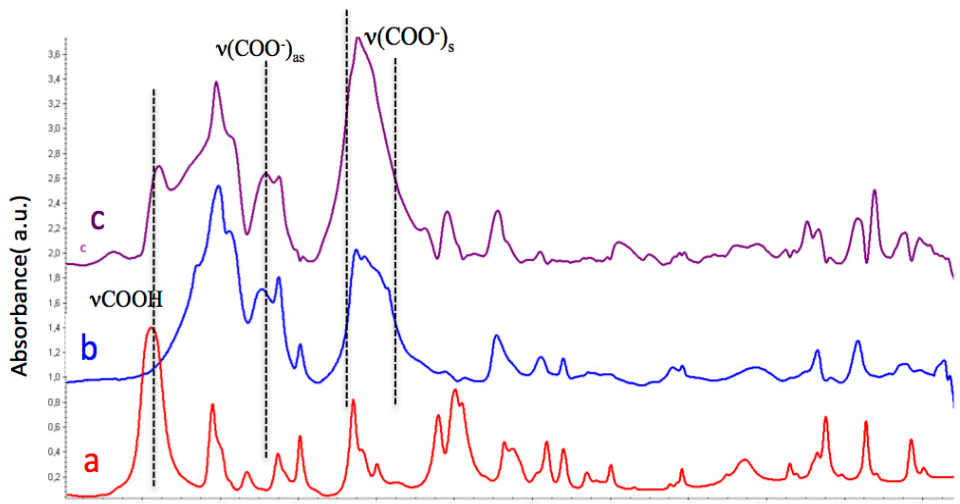


Figure 7: I IR spectrum of (a) the free acid in KBr (b) of molecules grafted on ZnO NPs powder in KBr and (c) PM-IRRAS spectrum of $\text{CH}_3\text{O-PP-COOH/ZnO/Au}$; II idem for F-PP-COOH/ZnO/Au ;III Geometrical sketch of oriented molecule with the orientation parameters

3.1.2 PM-IRRAS Spectra

In order to obtain the relative intensities of the dipolar transition moments of the grafted molecules and thus the molecular orientation, we determined the IR spectra of the molecules grafted isotropically onto a powder of ZnO nanoparticles.

Figure 7.I compares the PM-IRRAS spectra of $\text{CH}_3\text{O-PP-COOH/ZnO}$ film deposited on a gold substrate with the IR absorption spectra of the molecules free or grafted onto ZnO NPs, both in

KBr. We deduce that the molecules are grafted onto the ZnO surface, since the band assigned to COOH at 1681 cm⁻¹ is no longer present in either spectrum of the molecules with ZnO. The acid function has evolved into a carboxylate anion bound to the Zn(II) cation, which gives two new bands. A broad symmetric one, $\nu(\text{COO}^-)$, at 1426 cm⁻¹ (1425 cm⁻¹ for ZnO NPs), polarized along the bisectrix of the OCO angle, and a weak asymmetric one at 1545 cm⁻¹ (1549 cm⁻¹ for ZnO NPs), polarized perpendicularly to the previous band.

The $\nu_1(\text{C}=\text{C})$ biphenyl band is blue-shifted from 1599 cm⁻¹ to 1606 cm⁻¹ and the biphenyl $\nu_2(\text{C}=\text{C})$ band red-shifted from 1530 to 1527 cm⁻¹ (1526 cm⁻¹ for ZnO NPs) (Table1).

The main vibration modes of CH₃O-A in a KBr pellet are reported in Table 1 and compared to DFT values computed at the B3LYP/6-31+G* level. The frequencies differ by 0-10 cm⁻¹.

The nature of the chemisorption of a carboxylic acid on a metal oxide strongly depends on the difference $\Delta(\nu\text{COO}^-) = \nu(\text{COO}^-)_{\text{as}} - \nu(\text{COO}^-)_{\text{s}}$ [32,33]. The value of $\Delta(\nu\text{COO}^-) = 120 \text{ cm}^{-1}$ indicates that grafting occurs by bidentate bridging with two oxygen atoms bonded symmetrically to two Zn²⁺ atoms.

The PM-IRRAS spectra of F-PP-COO⁻/ZnO/Au (Fig.7 II) shows that F-A has been ~~successfully~~ grafted onto the ZnO surface, since the band assigned to $\nu(\text{COOH})$ at 1689 cm⁻¹ has disappeared. There is a weak asymmetric band $\nu(\text{COO}^-)$ at 1542 cm⁻¹. The $\nu_1(\text{C}=\text{C})$ band of biphenyl is red-shifted from 1609 to 1605 cm⁻¹ (1603 cm⁻¹ for ZnO NPs) while the $\nu_2(\text{C}=\text{C})$ band of biphenyl at 1525 cm⁻¹ does not move.

Similarly, for F-A the experimental wavenumbers are lower than the theoretical ones by ca. 10-25 cm⁻¹ (Table 1). The value of $\Delta(\nu\text{COO}^-) = 118 \text{ cm}^{-1}$ is consistent with grafting again involving bidentate bridging with two oxygen atoms bonded symmetrically to two Zn²⁺ atoms.

3.1.3 Molecular orientation

Using the relative absorbance ratio of the transition bands in the SAM/ZnO ($I(L_{1607})/I(M_{1528})$) and ($I(M_{1528})/I(N_{830})$), and by comparison with those corresponding to molecules in KBr ($A(L_{1607})/A(M_{1528})$) and ($A(M_{1528})/A(N_{830})$), we can estimate the orientation of the two molecules as follows. By using the selection rule for a metallic substrate we get:

$$\text{Abs} \propto \left| \vec{M} \cdot \vec{E} \right|^2 \quad (1)$$

Where \vec{M} is the transition dipolar moment, and \vec{E} is the electrical field perpendicular to the metallic gold substrate. Let us point out that the computed angle of inclination with respect to the normal to the surface of gold is overestimated compared to the real angle, with the local normal towards the not fully flat surface of ZnO NP that is concerned by the variation of the work function.

From equation (1) we can determine the tilt and twist angles, α and β , respectively (Fig. 7.III, table 2), by the following equations [34]:

$$\beta = \text{Arc tan} \sqrt{\frac{I_N \cdot A_M}{I_M \cdot A_N}}, \quad \text{tg} \alpha = \frac{1}{\cos \beta} \sqrt{\frac{I_M \cdot A_L}{I_L \cdot A_M}} \quad (2)$$

For CH₃O-A, in order to measure correctly the angles of orientation, the M and L bands were deconvolved .

Molecules	CH ₃ O-A	F-A
Angles		
$\alpha(^{\circ})(\pm 5)$	56	26
$\beta(^{\circ})(\pm 5)$	41	46

Table 2: Estimation of the orientation angles of the molecules (SAMs) ; the tilt angle is here slightly overestimated (see text).

According to the IR spectra, the tilt angle of F-A is smaller than that of CH₃O-A. Since the tilt angle determines the effect of the dipole and the variation of the work function, we can infer that the effect of the dipole of F-A is enhanced relatively to CH₃O-A.

3.2. Characterization by contact angle measurements: Determination of surface and adhesion energy

The outermost part of the SAMs/ZnO layers is chemically important since it determines the way of growth and organization of the photoactive P3HT-PCBM blend. We have probed this by measuring the wetting of the SAMs and their adhesion energy with organic SC. For the F-A/ZnO

sample, the contact angle reaches a maximum value of 103°, which shows that the layers are well organized (Table 3). This result is similar to that found in the literature for a hydrophobic molecule with fluorine [27].

surface	Contact angle (°)	
	Water	Diiodomethane
ZnO	47	60
CH ₃ O-A/ZnO	62	52
F-A/ZnO	103	45

Table 3: Measurement of the contact angle of ZnO and of different SAM-modified ZnO surfaces.

Surface energy values were derived from the contact angles. The surface energy (γ) components are calculated according to the method of van Oss, Good and Chaudhury [35]. We determined the adhesion energy ($W_{\text{ZnO-M}}$) of ZnO modified with P3HT et PCBM, considering that it consists of two components resulting from dispersive ($W_{\text{ZnO-M}}^d$) and polar ($W_{\text{ZnO-M}}^p$) interactions ($M = \text{P3HT or PCBM}$). Thus, $W_{\text{ZnO-M}}$ is considered as the sum of two terms:

$$W_{\text{ZnO-M}} = W_{\text{ZnO-M}}^d + W_{\text{ZnO-M}}^p \quad ; \quad W_{\text{ZnO-M}}^p = 2\sqrt{\gamma_{\text{ZnO}}^p \cdot \gamma_M^p} \quad W_{\text{ZnO-M}}^d = 2\sqrt{\gamma_{\text{ZnO}}^d \cdot \gamma_M^d}$$

$$W_{\text{ZnO-M}} = 2(\sqrt{\gamma_M^d \cdot \gamma_{\text{ZnO}}^d} + \sqrt{\gamma_{\text{ZnO}}^p \cdot \gamma_M^p})$$

The two components resulting from dispersive (γ_M^d) and polar (γ_M^p) interactions to the surface energies of P3HT and PCBM are determined from the literature [36].

The physicochemical properties of the groups F and CH₃O, and the differences in orientation, result in a lower polar component of the surface energy for the former than for the latter, 0.4 and 8 J/m², respectively, while the dispersive components are similar (Table 4).

The adhesion energies of P3HT with CH₃O-A/ZnO (78 J/m²) and bare ZnO (79 J/m²) are close but larger than those for F-A/ZnO (70 J/m²). Identically, PCBM also interacts the most with CH₃OSAM (106 J/m²) and ZnO (111 J/m²). On the other hand, the FSAM surface appears the less interacting and in this case, the interactions of P3HT and PCBM are both optimum with PCBM, 72 J/m² and 100 J/m² respectively with however strongest PCBM-PCBM interactions. Clearly, CH₃OSAM and bare ZnO interact more strongly with the photoactive molecules than F-A.

Sample	Surface energy (J/m ²)			Energy of cohesion or adhesion (J/m ²) with		Strongest interaction of the blend P3HT and PCBM components when in contact with the three surfaces (J/m ²)
	Total	Dispersive	Polar	P3HT	PCBM	
P3HT	26.9	24.6	2.3	54	72	
PCBM	50.2	39.8	10	72	100	
ZnO	62	45	17	79	111	P3HT-ZnO 79 PCBM-ZnO 111
CH ₃ O _{SAM} /ZnO	57	49	8	78	106	P3HT-CH ₃ O _{SAM} 78 PCBM-CH ₃ O _{SAM} 106
F _{SAM} /ZnO	47	46.6	0.4	70	90	P3HT-PCBM 72 PCBM-PCBM 100

Table 4: Measurement of the surface, adhesion and interaction energies.

Comparing the two SAMs, we expect that with CH₃OSAM, the surface interactions drive the first step of the deposition whereas with FSAM, the interactions in solution are predominant. Another consequence with the fluorinated SAM is the higher mobility of the weakly adsorbed photoactive molecules; this mobility may promote the aggregation notably of PCBM at the

FSAM surface . On the other hand , the methoxy SAM may ensure an initial random distribution of adsorbed interpenetrated photoactive molecules .

It appears difficult at this stage to establish a clear relationship between the interactions at the surface and the structuration of the heterolayers . We expect at least some differences in the organization and interpenetrations of P3HT and PCBM phases [37].

Let us point out that the films observed with binocular magnifiers, are a little more homogeneous with the CH3OSAM than with FSAM as may be expected from previous consideration. This point will be clarified thanks to the electrical analysis below .

4. Electrical characterization of the photovoltaic cells

Figure 8 shows the current density versus applied voltage J-V characteristic in the dark for the FTO/ZnO/P3HT-PCBM/PEDOT/Au cells, the ZnO being treated by SAMs or not.

These characteristics show a rectifying character except for F-A/ZnO. The current through the samples is quite high (of the order of mA/cm²). For CH₃O-A, the dipole *a priori* oriented (- +) from the ZnO towards the active film ($m < 0$) lowers the work function of the ZnO, so the difference between the LUMO of the PCBM (Acceptor) and the conduction band of the ZnO decreases, leading to an improvement in the internal field and to the rectifying effect. For F-A grafted onto ZnO, the dipole oriented (+ -) from the ZnO towards the active film ($\mu > 0$), leads to a significant increase in the work function of the ZnO and contributes to the reduction of the built-in field. This accounts for the quasi-symmetrical behavior of the I-V curve in the dark (see 4.2)

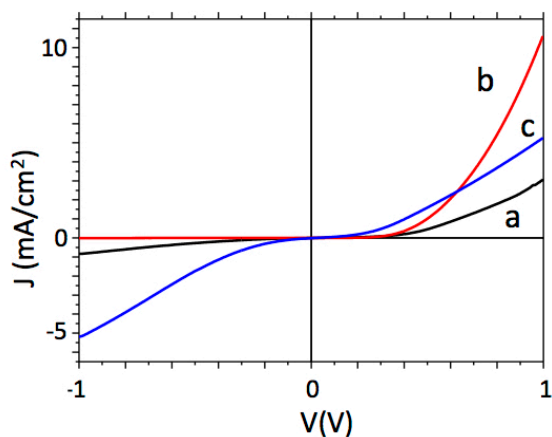


Figure 8 : Current density-voltage J-V curves of inverted OSCs in the dark: (a) ZnO; (b) CH3OSAM/ZnO; (c) FSAM/ZnO

4.1. Photoelectric parameters of the cells

The J-V curves (Fig. 9) recorded under white light illumination confirm the diode-like photovoltaic behavior of our samples with significant rectification, together with a short-circuit current density of the order of some mA/cm² and an open-circuit voltage varying between 0.19 and 0.5 V for all ZnO samples. As shown in Table 5, the values of the open-circuit voltage of the cells with F-A/ZnO, ZnO and CH₃O-A/ZnO are 0.19, 0.39 and 0.50 V, respectively. The structure with CH₃O-A shows the best value of V_{oc} . On the contrary, for F-A, the value of V_{oc} is much lower than that for bare ZnO. The improvement of the V_{oc} for CH₃O-A and noticeable reduction for F-A would suggest *a priori* a significant dipole effect (see Discussion).

The values of the short-circuit current density (J_{sc}) of the cells with F-A, ZnO and CH₃O-A are 5.8, 8.7 and 9 mA/cm², respectively. The structure with CH₃O-A has a J_{sc} very similar to that of bare ZnO. On the other hand, the J_{sc} value for F-A is lower than for untreated samples.

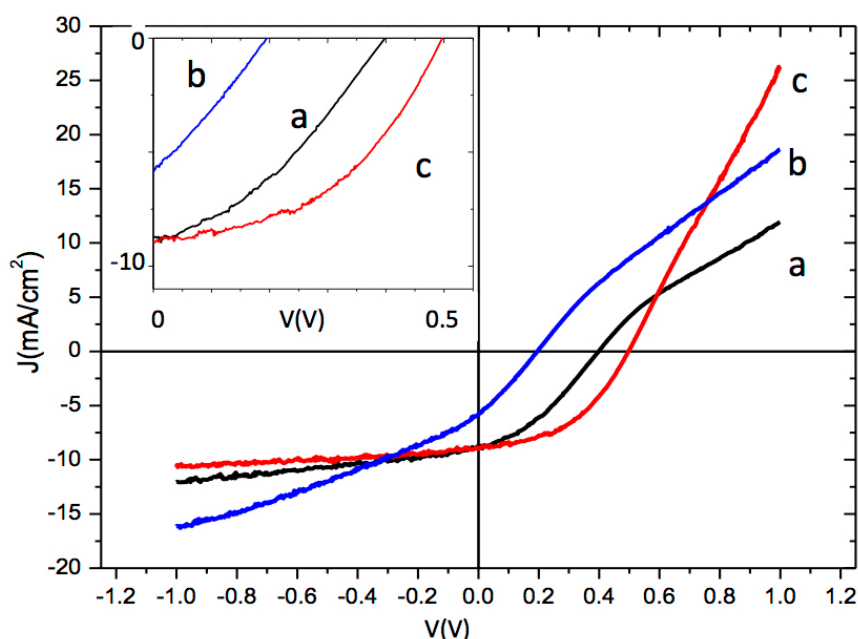


Figure 9: Current density-voltage J-V curves of inverted OSCs under AM 1.5 G simulated illumination with an intensity of 65 mW/cm²: (a) ZnO; (b) CH₃OSAM/ZnO; (c) FSAM/ZnO. Inset : zoom on the area of photovoltaic interest

The shapes of the J-V curves are strongly affected by the SAMs. Notably a low value of the fill-factor (FF) of the cell is obtained with F-A/ZnO (27%) whereas bare ZnO and CH₃O-A/ZnO have FF values of 35% and 45%, respectively.

Sample	V_{oc} (V)	J_{sc} (mA/cm ²)	FF(%)	PCE(%)	$r_{sep} = J_{Lmax}/J_{ph,sat}$ (%)	R_p (Ω.cm ²)	R_s (Ω. cm ²)
ZnO	0.39	8.7	35 (s*)	1.8	49	168	30
CH ₃ O-A/ZnO	0.50	9	45	3.1	54	324	20
F-A/ZnO	0.19	5.8	27 (s*)	0.45	27	46	29

Table 5: Photovoltaic parameters for cells with and without SAM; (s*: s-shaped curve).

Another striking feature in the I-V curves for bare ZnO and F-A/ZnO under illumination is their s-shaped form. In the first case, this behavior is most likely a direct consequence of the phenomenon of recombination of free charges or of a charge transfer complex at the surface states of ZnO [38]. The holes created at this interface can recombine easily with the electrons via the surface states of ZnO and this induces the s-shaped behavior and therefore a lower FF. These surface states, often associated with pendant links, are suppressed by the presence of a SAM. This phenomenon should in principle also intervene with F-A, but this is clearly not the case. This unexpected behavior may result from the negatively charged plane containing the fluorine, which attracts the minority carriers (holes) towards the ZnO layer and then increases hole-electron recombination.

The PCE values for cells with F-A/ZnO, bare ZnO and CH₃O-A/ZnO are 0.4, 1.8 and 3.1%, respectively. The best performance is obtained understandably with CH₃O-A/ZnO. The fluorinated SAM leads to a much lower value than bare ZnO. These solar cells present a PCE twice as large with an adequate SAM. The PCE are comparable to those found in the literature [39,40].

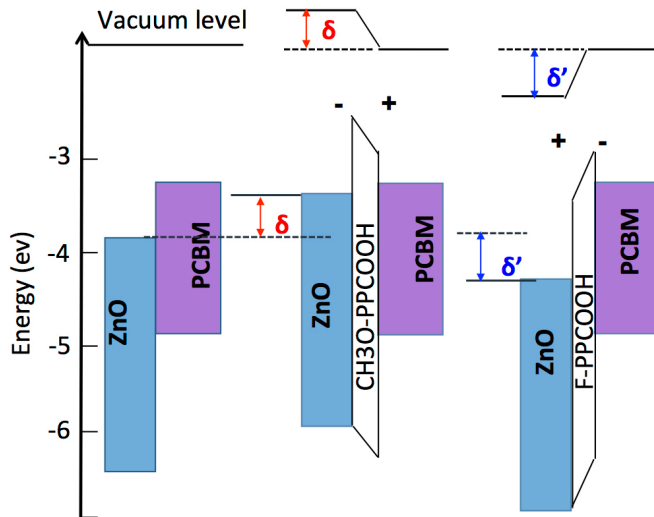


Figure 10: Energy level diagram of the devices with SAM-modified ZnO.

Low values of parallel resistance R_p (or shunt resistance), obtained from the inverse of the slope of the J-V curve at J_{sc} , account for a large leakage current independent of photoabsorption. We observe a large difference of R_p between $\text{CH}_3\text{O-A/ZnO}$, bare ZnO and F-A/ZnO cells, which have the following values, 330, 170 and 50 $\Omega\cdot\text{cm}^2$, respectively. The best and largest R_p value is obtained with $\text{CH}_3\text{O-A/ZnO}$, 50% greater than for bare ZnO, which is itself 400% higher than that for F-A/ZnO. For the latter the smaller R_p involves a large leakage current (Table 5).

The values of the series resistance, R_s , which is the inverse of the slope of J-V curve at J_{sc} and accounts for the resistance of the contacts, are similar for the SAM-based cells and greater than for bare ZnO (30 $\Omega\cdot\text{cm}^2$).

4.2. Analysis of results

The value of V_{oc} improves on going from bare ZnO and $\text{CH}_3\text{O-A/ZnO}$ -based cells (from 0.39 to 0.50 V), whereas the J_{sc} values are the same and the R_p values are comparable. V_{oc} varies independently of the current density J_{sc} and only accounts for the energy shift at the ZnO/P3HT-PCBM interface. Clearly the presence of the dipolar $\text{CH}_3\text{O-A}$ diminishes the work function of ZnO and increases V_{oc} (see below).

The bulk microstructure of the P3HT-PCBM blend affects the J_{sc} . We deduce that bare ZnO and $\text{CH}_3\text{O-A/ZnO}$ induce similar microstructuration of the blend [41-43].

On the other hand, F-A decreases V_{oc} ($\Delta V_{oc} = -0.2$ V), J_{sc} ($\Delta J_{sc}/J_{sc} = -35\%$) and R_p ($\Delta R_p/R_p = -75\%$) compared to bare ZnO. In this case, the SAM has an effect not only on the reduction of V_{oc} but also negatively affects the microstructure blend.

To analyze the issue of the effect on blend morphology, we consider (i) the neat photocurrent density (J_{ph}), which is expressed by the difference between the currents under illumination (J_L) and in the dark J_D ($J_{ph} = J_L - J_D$) and (ii) J_{Lmax} which is the current density at the point of maximum power. J_{ph} reaches a plateau with a saturation current density $J_{ph,sat}$. According to [41], the a relevant parameter with respect to a good phase separation is the value of the ratio $r_{sep} = J_{Lmax}/J_{ph,sat}$. As observed from Table 5, r_{sep} reaches similar values of 49% and 54% with ZnO and CH₃O-A/ZnO whereas the ratio falls to 27% with F-A/ZnO.

Thereby we expect a large difference of phase segregation and interpenetration of the blend as suggested above (see 3.2) i.e. a good phase separation in the first cases and in the second case of the fluorinated molecule, large-scale heterogeneities and too large domains to lead efficient exciton dissociation.

Therefore, the increase of V_{oc} observed with CH₃O-A/ZnO can be attributed to a dipole effect. Conversely, the V_{oc} drop from 0.39 to 0.19 V with F-A/ ZnO can not only be attributed to such an electrostatic effect of the SAM, but also reflects a variation of the structural order of the active mixture developed on the SAM having low surface energy. This unfavorable structuration, with domains bigger than the diffusion length in the case of F-A, which limits the exciton dissociation at the P3HT-PCBM interface and increases the recombination probability, has been pointed out previously [42].

4.3. Semi-Quantitative meaning of the dipole effect

For CH₃O-A, the dipole oriented (- +) from the ZnO towards the active film ($\mu_M < 0$) lowers the work function of the ZnO, so the difference between the LUMO of the PCBM and the conduction band of the ZnO decreases, leading to an improvement in the internal field and an increase in V_{oc} respectively [43, 44]: (+0.11 V) (10. 9). This also accounts for the increase in conversion efficiency from 1.2% to 2%. For F-A grafted onto ZnO, the dipole μ_M , oriented (+ -) from the ZnO towards the active film (> 0), leads to a significant increase in the work function of the ZnO and contributes to the reduction of V_{oc} (-0.2 V).

The maximum V_{oc} is generally expressed as the difference between the HOMO of the donor and the LUMO of the acceptor. However, misalignment of the electronic levels of the electrodes and

those of the active molecules decreases V_{oc} . The open-circuit voltage is given by the following equation, which takes into account the density of charges g_{PEDOT} and g_{ZnO} photogenerated at the anode and the cathode, respectively [45]:

$$V_{oc} = \frac{1}{e} \left((\phi_{PEDOT} - \phi_{ZnO}) + \Delta\phi \right) - \frac{kT}{e} \ln \left(\frac{g_{PEDOT}}{g_{ZnO}} \right) \quad (3)$$

where the potential energy shift $\Delta\phi$ due to a dipolar SAM layer (μ_M) at the ZnO surface is given by [46]:

$$\Delta\phi = \frac{e\Gamma\mu_M}{\epsilon_r\epsilon_0} \quad (4)$$

Here Γ is the surface density of SAM molecules, which may depend on the nature of the grafted molecule, e (> 0) the elementary charge, μ_M the dipole moment of the adsorbed molecule considered as positive when it is directed (+ -) from FTO/ZnO to PEDOT/Au, ϵ_0 is the vacuum permittivity and ϵ_r the static dielectric constant of the SAM layer.

In our previous work [45], we took into account photogeneration at the anode and cathode interfaces, since the structure was far from a BHJ. However, in the present case one can assume that the main photogeneration process takes place in the bulk, far from the electrode interfaces, which leads to the neglect of the latter term in equation (3); the open-circuit voltage can then be expressed by the following equation :

$$V_{oc} = \frac{1}{e} \left((\phi_{PEDOT} - \phi_{ZnO}) + \Delta\phi \right) \quad (5)$$

Considering the work functions of ZnO and PEDOT:PSS as 4.0 ± 0.1 and 4.33 ± 0.1 eV, respectively, we note that our experimental value of $V_{oc} = 0.39$ V is slightly greater than that derived from the difference between the work functions of the electrodes (0.33 ± 0.2 V), which is: $1/e (\phi_{PEDOT} - \phi_{ZnO}) \geq 0.39 \pm 0.1$ V. Indeed, the work function of ZnO, W_{ZnO} , should be reduced by 0-0.06 eV, i.e. it is between 4 and 3.94 eV.

4.4. Estimation of the grafting dipole

The best V_{oc} was obtained with $CH_3O-PP-COOH$. The difficulty in applying equation (2) comes from the lack of knowledge of $\Delta\phi$ or of the dipole moment of the grafted molecule. Indeed, the overall dipole implies several components. The first is due to the neutral moiety with the

methoxy group and the second is induced by the grafting and formation of (COO⁻, ZnOH⁺ or COO^{δ-}-ZnOH^{δ+}).

Cornil *et al.* have extensively addressed this calculation with a grafted SAM, Y-P-COOH/ZnO (Y = CH₃O, H, CN) [47]. They decompose the variation of the total work function for bare ZnO, $\delta W_{\text{DFT}}(\text{eV})$, into three components related to: i) the core of the molecule (or its radical F-A[•]); ii) the ZnO modification (rZnO), and iii) bond-dipole potential (BD):

$$\delta W_{\text{DFT}}(\text{SAM}) = \delta W_{\text{rYPCOO}} + \delta W_{\text{rZnO}} + \delta W_{\text{BD}} \quad (6a)$$

The rZnO part is weak and does not depend on Y (± 0.05 eV) and very little on the grafting mode. The BD part is rather important but depends a few on Y. Then for a set of molecules having the same grafting mode, we may expect:

$$\delta W_{\text{DFT}}(\text{SAM}) \approx \delta W_{\text{rYPCOO}} + \text{constant} \quad (6b)$$

Figure 11 shows the total variation of the work function of the ZnO grafted molecules, $\delta W_{\text{DFT}}(\text{eV})$, as a function of the calculated (eq. 7) work function for the neutral SAM (nSAM) or a physisorbed one, $\delta W_{\text{nYPCOOH}}$. This curve appears linear with a slope of 0.99 with an attenuation of the effect of the dipole of the neutral molecule on δW_{DFT} due to the grafting on ZnO. This should reflect the validity of equation 6b. A similar model has been evaluated and compared with experimental data obtained by UPS or Kelvin probe [48].

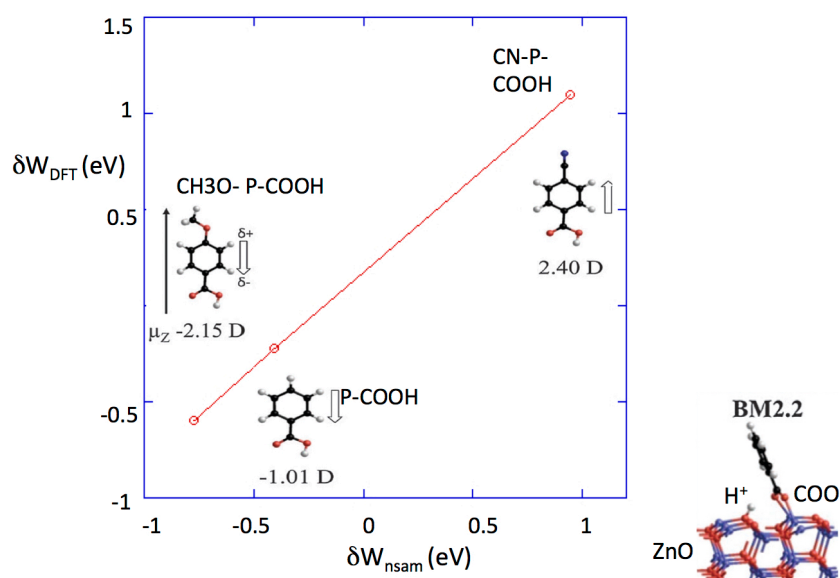


Figure 11: Variation of the work function δW_{DFT} of acid molecules grafted onto ZnO via BM2-2 mode (bidentate) as a function of that of the neutral acids deduced from their dipole moment μ_M (Debye) (eq. 7); see text and [47]

Concerning F-A and CH3O-A molecules, the same bidentate grafting is supported by the fact that the difference in wavenumbers, $\nu\text{COO}^-(\text{as})-\nu\text{COO}^-(\text{s})$, is equal for the two molecules (118 cm^{-1} for FA and 117 cm^{-1} for CH3O-A). Given the similarity between the monophenyl molecules with biphenyl ones and notably assuming an identical grafting, we may apply the quasi-linear relation between $\delta W_{\text{DFT}} = f(\delta W_{\text{NYPPCOOH}})$, for the grafted SAM of CH3O-A.

we have :

$$\delta W_{\text{nSAM}}(\text{eV}) = \delta V(\text{volt}) = \Gamma_{\text{nSAM}} * \mu\text{M} * \cos(\alpha) * 3,77 \cdot 10^{-19} / \epsilon_{\text{nSAM}} \quad (7)$$

$$\delta W_{\text{nCH3OA}} = -0.58\text{ eV}$$

the calculated dipole μM by DFT is -2.94D ; Γ_{nSAM} is the density of molecules estimated via the area projected on the surface, α the tilt angle already calculated by IR, ϵ_{nSAM} is the static dielectric constant of the nSAM, estimated at 4.2; the latter is estimated by the calculated dipole moment of the radical CH3O-P \cdot (5.7 D) and $\delta W_{\text{rCH3OP}\cdot}$ found in Cornil et al. The surface densities of two molecules were estimated by modeling the molecules in blocks:

$$\Gamma_{\text{nCH3O-A}} = 3,95 \cdot 10^{14}\text{ mol/cm}^2 \text{ and } \Gamma_{\text{nF-A}} = 4.2 \cdot 10^{14}\text{ mol/cm}^2.$$

For the F-A molecule with its dipole of -0.15D , we obtain $\delta W_{\text{nF-A}} = -0.054\text{ eV}$ using the previous relation ($\epsilon_{\text{nFA}} = 4$, $\alpha = 26^\circ$) (table 6). From the curve in fig. 11, we get by extrapolation the δW_{DFT} values of -0.41 and 0.11V for the two grafted SAMs.

	Dipole moment of neutral molecules (Debye)	δW_{nSAM} (eV)	$\delta W_{\text{DFT, (SAM)}}$ (eV)	δV_{oc} eff (in presence of PCBM) (V)	δV_{oc} (SAM-ZnO) (exp.) (V)	δV_{oc} (SAM-ZnO)- δV_{oc} eff (V)
ZnO	0	0	0			
CH ₃ O-A	-2.94	-0.58	-0.41	≥ 0.13	0.11	-0.02
F-A	-0.15	-0.053	0.11	-0.11	-0.20	-0.09

Table 6: Comparison of theoretical and experimental V_{oc} values for bare ZnO and SAM-modified ZnO.

Indeed, the value of $-\delta W_{\text{DFT}}(\text{CH}_3\text{O-A})$ is larger than the difference between the Conduction Band (CB) of ZnO and the LUMO of PCBM (3.7 eV), which is an unusual case, rarely treated in the literature. A dipolar effect of around 0.3 eV (or 0.3 V), i.e. equal to the difference between the CB of the ZnO and the LUMO of the PCBM ($W_{\text{LUMO PCBM}}$), would be ideal to obtain the alignment between the levels of ZnO (W_{CBZNO}) and PCBM. An excessive dipolar effect should induce electron transfer from ZnO to the LUMO of PCBM provided that the ZnO is sufficiently doped. This restores the energetic equilibrium and the electronic structure of the PCBM with respect to ZnO.

The relative positions of the CB_{ZnO} and the $\text{LUMO}_{\text{PCBM}}$ determine whether there is an extraction barrier or not. An extraction barrier expected here with undoped ZnO (necessarily less than 0.14 eV) should induce carrier recombination and therefore a decrease in V_{oc} . Clearly, this loss of potential cannot be higher than 0.14 V relative to the ideal alignment (loss = 0) and we expect for the effective value of δV_{oc} in presence of PCBM:

$$\delta V_{\text{oc,eff}}(\text{CH}_3\text{O-A})(\text{V}) \geq 2(W_{\text{CBZNO}} - W_{\text{LUMO PCBM}}) + \delta W_{\text{DFT}}(\text{CH}_3\text{O}) (\text{V}) = 0.13 \text{ V} \quad (\text{see fig.12})$$

We note that the estimated value of 0.13 V obtained with CH₃O-A is quite close to the experimental value, suggesting that the dipole effect accounts for the value of V_{oc} . In the case of F-A, the experimental variation of $|V_{\text{oc}}|$ relative to bare ZnO is higher than the semi-calculated value ($|-0.11 \text{ V}|$). The effect of F-A seems to be more damaging than expected for the dipole effect alone. This confirms that another effect is involved in the loss of performance of the devices with F-A. As shown before, the poor performance of the OSC, i.e. the decrease in J_{sc} , $J_{\text{Lmax}}/J_{\text{ph,sat}}$ and PCE, has been observed and accounted for by the nature of the microstructuring. Consequently, the impact of F-A is not entirely due to a dipole electrostatic effect.

In conclusion, the dipolar effect of CH₃O-A has been evidenced semi-quantitatively and is related mainly to the improvement of V_{oc} . The SAM has no significant influence on J_{sc} and thus on the structure of the photoactive film. On the other hand, the lowering of J_{sc} , V_{oc} and the overall performance of the PV cell observed with F-A are accounted for by the dipole effect and the nanostructuring of the photoactive film.

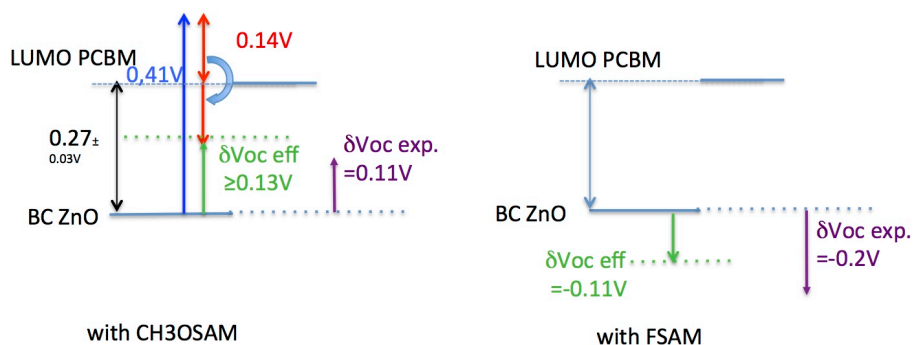


Figure 12. Effect of the two SAMs on the displacement of conduction band of ZnO towards the LUMO of PCBM and on the variation of V_{oc} relatively to bare ZnO

5. Conclusion

The modification of ZnO by two SAMs, CH₃OSAM and FSAM, reveals large differences in the interface properties, active film structuration and overall PV performance of the cells. However, the influence of the SAM is very dependent on its nature, orientation, and wettability. When ZnO is treated with CH₃O-A, the cell V_{oc} improves and the total PCE is twice as high as for bare ZnO. On the other hand, FSAM decreases both V_{oc} , J_{sc} and the PCE, which is reduced by a factor of four with respect to bare ZnO. Comparison of the features of CH₃OSAM and FSAM allows us to clearly distinguish two possible effects: (i) on the work function of ZnO via the dipole; (ii) on the P3HT-PCBM blend microstructure.

In the case of CH₃OSAM, the effect of the calculated dipole on the variation of the ZnO working function - even with a weakly defined molecule orientation - is large and even greater than the difference between the electronic levels of the LUMO_{PCBM} and the CB_{ZnO}. The V_{oc} is better than with the bare ZnO. The wetting of CH₃OSAM and its adhesion with the blend are quite similar to those of bare ZnO, and in the same way, the current densities are very close. Consequently, the microstructurations are also quite similar and the SAM dipole effect only is important on V_{oc} . The well-oriented FSAM, with its inverted dipole compared to CH₃OSAM, negatively affects the variation of the work function of the oxide. However, V_{oc} and J_{sc} are both reduced. The inadequate microstructuring of the photoactive mixture, due to the poor wetting of the FSAM, and the weakness of its interaction with the blend components, is also involved in the poor overall performance of the OPV cell.

Acknowledgments:

We thank very much Pr. Antoine Kahn for his remarks and the stimulated discussions. Similarly, we are grateful to Dr. John Lomas (CNRS DR) for his proofreading and text enhancements. Quantum chemical calculations were performed using HPC resources from GENCI- [CCRT/CINES/IDRIS] (Grant 2019[A0080807006]).

References

- [1] C. J. Brabec, N. S. Sariciftci, J. C. Hummelen, Plastic Solar Cells, *Adv. Funct. Mater*, 11(1) (2001) 15–26.
- [2] J. Y. Kim, K. Lee, N. E. Coates, D. Moses, T. Q. Nguyen, M. Dante, A. J. Heeger, Efficient tandem polymer solar cells fabricated by all-solution processing, *Science*, 317 (5835) (2007) 222–225.
- [3] R. H. Friend, R. W. Gymer, A. B. Holmes, J. H. Burroughes, R. N. Marks, C. Taliani, D. Bradley, D. A. Dos Santos, J. L. Bredas, M. Lögdahl, W. R. Salaneck, Electroluminescence in conjugated polymers, *Nature*, 397 (6715) (1999) 121–128.
- [4] S. E. Shaheen, C. J. Brabec, N. S. Sariciftci, 2.5% Efficient Organic Plastic Solar Cells, *Appl. Phys. Lett.* 78, (6) (2001) 841–843.
- [5] G. Li, V. Shrotriya, J. S. Huang, Y. Yao, T. Moriarty, K. Emery, Y. Yang, High-efficiency solution processable polymer photovoltaic cells by self-organization of polymer blends, *Nature Materials* 4(11) (2005) 864–868.
- [6] W. Ma, C. Yang, X. Gong, K. Lee, A. J. Heeger, Thermally Stable, Efficient Polymer Solar Cells with Nanoscale Control of the Interpenetrating Network Morphology, *Adv. Funct. Mater*, 15(10) (2005) 1617 – 1622.
- [7] J. Peet, J. Y. Kim, N. E. Coates, W. L. Ma, D. Moses, A. J. Heeger, G. C. Bazan, Efficiency enhancement in low-bandgap polymer solar cells by processing with alkane dithiols, *Nat. Mater*, 6(7) (2007) 497–500.
- [8] W. Y. Wong, X. Z. Wang, Z. He, A. B. Djurisic, C. T. Yip, K. Y. Cheung, H. Wang, C. S. K. Mak, W. K. Chan, Metallated conjugated polymers as a new avenue towards high-efficiency polymer solar cells, *Nat. Mater*, 6 (7) (2007) 521–527.

- [9] F. C Krebs, Polymer solar cell modules prepared using roll-to-roll methods: Knife-over-edge coating, slot-die coating and screen printing, *Sol. Energy Mater. Sol. Cells*, 93 (4) (2009) 465–475.
- [10] S.I. Nia , S. S. Kim, S. S. Kwon, J. Jo, J. Kim, T. Lee, D. Y. Kim, Surface relief gratings on poly (3-hexylthiophene) and fullerene blends for efficient organic solar cells, *Appl. Phys. Lett*, 91 (17) (2007) 173509.
- [11] F.Liu, Y. Gu, J. W. Jung, W.Ho Jo,T. P. Russell, On the Morphology of Polymer-Based Photovoltaics *J. Polymer Science B : Polymer phys.* 50 (2012) 1018–1044
- [12] P. Kohn, Z. Rong, K. H. Scherer, A. Sepe, M. Sommer, P. Müller-Buschbaum, R. H. Friend, U. Steiner, S. Hüttner, Crystallization-Induced 10-nm Structure Formation in P3HT/PCBM Blends, *Macromolecules*, 46, (2013)4002–4013
- [13] F. Zhang, M. Ceder, O. Inganäs, Enhancing the Photovoltage of Polymer Solar Cells by Using a Modified Cathode, *Adv. Mater*, 19 (14) (2007) 1835–1838.
- [14] H. Choi, J. S. Park, E. Jeong, G. W. Kim, B. R. Lee, S. O. Kim, M. H. Song, H. Y. Woo, J. Kim, Combination of titanium oxide and a conjugated polyelectrolyte for high-performance inverted-type organic optoelectronic devices, *Adv. Mater*, 23 (2011) 2759–2763.
- [15] B. Wu, Z. Wu, Q. Yang, F. Zhu, T-W. Ng, C-S. Lee, S-H. Cheung, S-K. So, Improvement of Charge Collection and Performance Reproducibility in Inverted Organic Solar Cells by Suppression of ZnO Subgap States, *ACS Appl. Mater. Interfaces*, 8 (23) (2016) 14717–14724.
- [16] Z. Kam, Q. Yang, X. Wang, B. Wu, F. Zhu, J. Zhang, J. Wu, Enhanced absorbance and electron collection in inverted organic solar cells: optical admittance and transient photocurrent analyses, *Org. Electron*, 15 (7) (2014) 1306–1311.
- [17] Z. He, C. Zhong, S. Su, M. Xu, H. Wu, Y. Cao, Enhanced Power-Conversion Efficiency in Polymer Solar Cells Using an Inverted Device Structure, *Nat. Photonics*, 6 (9) (2012) 591–595.
- [18] H. Liu, Z. Wu, J. Hu, Q. Song, B. Wu, H. Tam, Q. Yang, W. Choi, F. Zhu, Efficient and ultraviolet durable inverted organic solar cells based on an aluminum-doped zinc oxide transparent cathode, *Appl. Phys. Lett*, 103 (4) (2013) 043309.
- [19] Y. Sun, H. Seo, C. Takacs, J. Seifert, A. J. Heeger, Inverted polymer solar cells integrated with a low-temperature-annealed sol-gel-derived ZnO Film as an electron transport layer, *Adv. Mater.* 23 (14) (2011) 1679–1683.
- [20] S. K. Hau, H-L. Yip, N. S. Baek, J. Zou, K. O'Malley, A. K.-Y. Jen, Air-stable inverted flexible polymer solar cells using zinc oxide nanoparticles as an electron selective layer, *Appl. Phys. Lett.* 92 (25) (2008) 253301.

- [21] B. A. MacLeod, B. J. Tremolet de Villers, Ph. Schulz, P. F. Ndione, H. Kim, A. J. Giordano, K. Zhu, S. R. Marder, S. Graham, J. J. Berry, A. Kahn, D. C. Olson, Stability of inverted organic solar cells with ZnO contact layers deposited from precursor solutions, *Energy Environ. Sci.*, 8 (2) (2015) 592–601.
- [22] S. Alem, J. Lu, R. Movileanu, T. Kololuoma, A. Dadvand, Y. Tao., Solution-processed annealing-free ZnO nanoparticles for stable inverted organic solar cells, *Org. Electronics*, 15(5) (2014) 1035-1042.
- [23] K. Sun, J. Ouyang; Polymer solar cells using chlorinated indium tin oxide electrodes with high work function as the anode, *Sol. Energy Mater. Sol. Cells*, 96, (2012) 238-243;
- [24] K Sun, B. Zhao, V. Murugesan, A. Kumar, K Zeng, J. Subbiah, W W. H. Wong, D J. Jones, J. Ouyang, High-performance polymer solar cells with a conjugated zwitterion by solution processing or thermal deposition as the electron-collection interlayer, *J. Mater. Chem.*, 22, (2012) 24155-24165;
- [25] M. J. Tan, S. Zhong, J. Li, Z. K. Chen, W. Chen, Air-Stable Efficient Inverted Polymer Solar Cells Using Solution-Processed Nanocrystalline ZnO Interfacial Layer, *ACS Appl. Mater. Interfaces*, 5 (2013) 4696-4701.
- [26] X. Jia, Z. Jiang, X. Chen, J. Zhou, L. Pan, F. Zhu, Z. Sun, S. Huang, Highly Efficient and Air Stable Inverted Polymer Solar Cells Using LiF-Modified ITO Cathode and MoO₃/AgAl Alloy Anode, *ACS Appl. Mater. Interfaces*, 8 (2016) 3792–3799.
- [27] Ye Eun Ha, M. Y. Jo, J. Park, Y-C. Kang, S. I. Yoo, J. H. Kim, Inverted Type Polymer Solar Cells with Self-Assembled Monolayer Treated ZnO, *J. Phys. Chem. C*, 117 (6) (2013) 2646–2652.
- [28] D. Jezequel, J. Guenot, N. Jouini, F. Fiévet, Submicrometer zinc oxide particles: Elaboration in polyol medium and morphological characteristics, *Journal of Materials Research*, 10 (1) (1995) 77-83.
- [29] R. Brayner, R. Ferrari-Iliou, N. Brivois, S. Djediat, MF. Benedetti, F. Fiévet, Toxicological impact studies based on *Escherichia coli* bacteria in ultrafine ZnO nanoparticles colloidal medium, *Nano Lett*, 6 (4) (2006) 866-870.
- [30] M. J. Frisch, G. W. Trucks, H. B. Schlegel, G. E. Scuseria, M. A. Robb, J. R. Cheeseman, G. Scalmani, V. Barone, B. Mennucci, G. A. Petersson, H. Nakatsuji, M. Caricato, X. Li, H. P. Hratchian, A. F. Izmaylov, J. Bloino, G. Zheng, J. L. Sonnenberg, M. Hada, M. Ehara, K. Toyota, R. Fukuda, J. Hasegawa, M. Ishida, T. Nakajima, Y. Honda, O. Kitao, H. Nakai, T. Vreven, J. A. Montgomery, Jr., J. E. Peralta, F. Ogliaro, M. Bearpark, J. J. Heyd, E. Brothers, K. N. Kudin, V. N. Staroverov, R. Kobayashi, J. Normand, K. Raghavachari, A. Rendell, J. C. Burant, S. S. Iyengar, J.

- Tomasi, M. Cossi, N. Rega, J. M. Millam, M. Klene, J. E. Knox, J. B. Cross, V. Bakken, C. Adamo, J. Jaramillo, R. Gomperts, R. E. Stratmann, O. Yazyev, A. J. Austin, R. Cammi, C. Pomelli, J. W. Ochterski, R. L. Martin, K. Morokuma, V. G. Zakrzewski, G. A. Voth, P. Salvador, J. J. Dannenberg, S. Dapprich, A. D. Daniels, Ö. Farkas, J. B. Foresman, J. V. Ortiz, J. Cioslowski, and D. J. Fox, *Gaussian 09* (Gaussian, Inc., Wallingford CT, 2009). Gaussian, Inc., Wallingford CT (2009).
- [31] C. Mihesan, M. Ziskind, C. Focsa, M. Seydou, F. Lecomte, J. P. Schermann, Structure of neat and hydrated liquid nicotine and laser resonant desorption of clusters from nicotine-water solutions, *International Journal of Mass Spectrometry*, 277 (1-3) (2008) 284-290.
- [32] Yu-Tai Tao, Structural comparison of self-assembled monolayers of n-alkanoic acids on the surfaces of silver, copper, and aluminum, *J. Am. Chem. Soc.*, 115 (10) (1993) 4350-4358.
- [33] M. Nara, H. Torii, M. Tasumi, Correlation between the Vibrational Frequencies of the Carboxylate Group and the Types of Its Coordination to a Metal Ion: An ab Initio Molecular Orbital Study *J. Phys. Chem*, 100 (51) (1996) 19812-19817.
- [34] H. Kim, Z. Meihui, N. Battaglini, Ph. Lang, G. Horowitz, Large enhancement of hole injection in pentacene by modification of gold with conjugated self-assembled monolayers, *Org. Electron.* 14, (2013), 2108–2113.
- [35] C. J. Van Oss, M. K. Chaudhury, R. J. Good, Interfacial Lifshitz-van der Waals and polar interactions in macroscopic systems, *Chem. Rev*, 88 (6) (1988) 927-941.
- [36] J-H. Huang, Y-S. Hsiao, E. Richard, C-C. Chen, P. Chen, G. Li, C-W. Chu, Y. Yang, The investigation of donor-acceptor compatibility in bulk-heterojunction polymer systems, *Appl. Phys. Lett*, 103 (4) (2013) 043304.
- [37] P. M. Beaujuge, J. M. J. Fréchet, Molecular Design and Ordering Effects in π -Functional Materials for Transistor and Solar Cell Applications, *J. Am. Chem. Soc*, 133 (50) (2011) 20009-20029.
- [38] A. Wagenpfahl, D. Rauh, M. Binder, C. Deibel, V. Dyakonov, S-shaped current-voltage characteristics of organic solar devices, *Phys. Rev. B*, 82 (11-15) (2010) 115306.
- [39] Y. Thaver, SO. Oseni, K. Kaviyarasu, RP. Dwivedi, GT. Mola, Metal nano-composite assisted photons harvesting in thin film organic photovoltaic, *Physica B: Condensed Matter*, 582(2020), 411844.
- [40] A. Hazra, I. Mal, D.P. Samajdar, T.D. Das, Analytical modelling of organic solar cells with scattering interface, *Optik*, 168 (2018) 747-753.
- [41] Y. Liu, D. Tang, Kaicheng Zhang, Peng Huang, Zhaowei Wang, Kai Zhu, Zhendong Li, Ligang Yuan, Jian Fan, Yi Zhou, Bo Song, Tuning Surface Energy of Conjugated Polymers via

Fluorine Substitution of Side Alkyl Chains: Influence on Phase Separation of Thin Films and Performance of Polymer, Solar Cells. *ACS Omega*, 2 (6) (2017) 2489–2498.

[42] W. Huang, E. Gann, L. Thomsen, A. Tadich, Yi-Bi. Cheng, Ch. R. McNeill, Metal Evaporation-Induced Degradation of Fullerene Acceptors in Polymer/Fullerene Solar Cells, *ACS Appl. Mater. Interfaces*, 8 (2016) 29608–29618.

[43] G. G. Malliaras, J. R. Salem, P. J. Brock, and J. C. Scott, Photovoltaic measurement of the built-in potential in organic light emitting diodes and photodiodes, *Journal of Applied Physics*, 84 (3) (1998) 1583.

[44] R. M. Hewlett, M. A. McLachlan, Surface Structure Modification of ZnO and the Impact on Electronic Properties, *Adv. Mater.*, 28(2016) 3893–3921

[45] F. Kouki, N. Karsi, P. Lang, G. Horowitz, H. Bouchriha, Effect of self-assembled monolayers on charge carrier photogeneration in sexithiophene based diodes, *Synthetic Metals* 162 (19-20) (2012) 1741–1745.

[46] S. Ray, H. Cohen, R. Naaman, Liu H. & D. Waldeck, Organization-Induced Charge Redistribution in Self-Assembled Organic Monolayers on Gold *J. Phys. Chem. B* 29 (2005) 129.

[47] D. Cornil, T. Van Regemorter, D. Beljonne, J. Cornil, Work function shifts of a zinc oxide surface upon deposition of self-assembled monolayers: a theoretical insight, *Phys.Chem.Chem. Phys.* 16 (38) (2014) 20887.

[48] H.Li, P. Winget, J.L. Bredas, Transparent Conducting Oxides of Relevance to Organic Electronics: Electronic Structures of Their Interfaces with Organic Layers *Chem. Mater.*, 26, (2014) 631–646

